# PREDICTION OF WAXY OIL DEPOSITION WITH DIFFERENT NON-NEWTONIAN MODELS

**Luis Renato Minchola Morán, luisminchola@aluno.puc-rio.br**
**Flavio Henrique Marchesini de Oliveira, fhmo@puc-rio.br**
**Bruna Câmara Trampus, bruna.trampus@yahoo.com.br**
**Angela O. Nieckele, nieckele@puc-rio.br**
**Luis Fernando A. Azevedo, lfaa@puc-rio.br**
**Paulo Roberto de Souza Mendes, pmendes@puc-rio.br**
Departamento de Engenharia Mecânica – Pontifícia Universidade Católica de Rio de Janeiro, PUC-Rio
R. Marques de São Vicente 225 – Rio de Janeiro, RJ, Brasil

***Abstract.*** *Wax deposition in the inner walls of pipelines is a critical problem for the petroleum industry due to the potential capital losses that it can cause. Indeed, paraffin deposition may lead to production loss, increased pumping power, elevated remediation costs and even loss of pipelines due to its total blockage. Below the wax appearance temperature (WAT), the solid wax particles leave the solution and they can alter the rheological properties of the fluid. At the present work the behavior of the flow and its influence in the deposit thickness is numerically investigated considering three different rheological models. To evaluate the models, the numerical results are compared with data obtained in well controlled experiment in a channel flow, employing a simple oil-paraffin. The fluid thermal physics properties and rheological parameters were experimentally determined. The finite volume method with a moving mesh adapted to the interface was applied to solve the conservation equations. The steady state deposit thickness presents a reasonable agreement with the experimental data. The jellification mechanism based on all three Non-Newtonian fluid models improved the transient prediction of the deposition rate, however, no model was clearly superior.*

***Keywords****: Wax Deposition, Molecular Diffusion, Non-Newtonian fluid, Numerical Simulation*

## 1. INTRODUCTION

Wax deposition is critical in offshore deep water production facilities where the flowlines are exposed to the cold ocean temperatures that prevail at elevated water depths. The warm oil exiting at approximately 60 ˚C from the well head looses heat to the surrounding environment at, typically, 4˚C as it flows to the production platforms. If the crude oil temperature falls below the Wax Appearance Temperature ($T_{WAT}$), the wax may precipitate and deposit along the inner walls of the pipeline.

Deposition of heavy paraffin molecules in the inner walls of pipelines is a serious problem for the petroleum industry due to the potential capital losses it can cause. Indeed, paraffin deposition, also termed wax deposition, may lead to loss of production, increased pumping power, elevated remediation costs and even loss of pipelines due to its total blockage. It is for that reason that there is a significant amount of publications with attempts of modeling this phenomenon. Most operators use simulation tools to predict the rate of wax deposition in pipelines. These models are employed in the design stages of the oil fields where the knowledge of the likelihood of occurrence of wax deposition is fundamental information that will influence the characteristics of the pipelines to be specified and, at the end, the cost of the future installation.

Molecular diffusion has been used as the wax deposition mechanism in the vast majority of the simulations available in the literature (Brown *et al*. 1993, Fusi 2003, Correra *et al*. 2007, Romero *et al*. 2006, Minchola *et al*. 2007). However, as stated by Azevedo and Teixeira 2003, there is still controversy related to the relevance of other deposition mechanisms. In recent years a number of studies have been published addressing different kinds of deposition mechanisms. Merino-Garcia *et al.* 2007 proposed the consideration of axial convective transport of liquid wax in solution, and the formation of the deposit as a gel structure at the pipeline wall, as a consequence of a phase change process. Mehrotra and Bhat 2007 proposed a one-dimensional cage model for the deposit where the composition of the deposit is determined by the hydrodynamic shear stress imposed by the flow. Minchola *et al.* 2008 presented a numerical simulation where Brownian diffusion of suspended wax crystals was included, together with molecular diffusion. Hoteit *et al.* 2008 developed a model where the wax-solvent fluid is considered as a multi-component mixture. The model is based on the coupled momentum, energy and species conservation equations and incorporates a term to account for Soret diffusion, whereby a thermal gradient induces mass transport. Attention has also been directed to the study of the composition of the solid deposit at the pipe wall.

Due to a large amount of solid wax particle present at temperature below $T_{WAT}$, the behavior of fluid can change from Newtonian to non-Newtonian. Since the rheological properties depend on cooling rate, share rate, and wax concentration, they are very difficult to be determined (Benallal *et al*. (2008) and Fasano *et al*. 2004).

Vinay *et al*. (2005) used an extension of the classical Bingham model in which plastic viscosity and yield stress are allowed to be temperature-dependent parameters. The viscous dissipation term was also included in the energy equation. A possible gel deposition by rheological properties is suggested by Benallal *et al*. (2008), who presented an

improvement in the Bingham and Herschel-Bulkley models, by introducing temperature and wax concentration dependency of the rheological parameters. An accurate work with the same methodology was presented by Ghanaei and Mowla (2010) combining the Herschel-Bulkley and Richardson model, with API, solid wax weight percent and shear rate dependence. To validate the model, some experimental data related to North Sea oils has been applied; the average error was 19.47%. Minchola *et al.* (2010) employed a model which combined a molecular-diffusion model with a temperature dependent Bingham fluid model for temperatures below the wax appearance temperature. Although there was no experimental data to validate the model, a good qualitative behavior of deposition thickness along the duct during the early stages of the deposition process was obtained.

The present paper is part of an ongoing research effort directed at identifying the relative importance of the mechanisms responsible for paraffin deposition. The research program encompasses experiments at the laboratory scale and numerical simulations. The experiments employ simple geometries with well defined and controlled boundary and initial conditions, using simple oil-wax solutions prepared in the laboratory, and with known transport properties. The results obtained from these controlled experiments are then compared to numerical simulations that try to faithfully reproduce the experimental conditions. Contrary to the experimental studies, the simulations studies permit that different models proposed for deposition mentioned in the literature can be tested individually, allowing, thereby, an assessment of the relative importance of each of the deposition mechanisms.

To investigate the influence of the rheological models in the wax deposition rate, the deposit thickness $\delta$ obtained with three different rheological models was compared with experimental data (Palomino, 2010), obtained in the test section schematically illustrated in Fig. 1a and 1b. Oil enters the domain, which has a rectangular cross section (height $a$ and width $W$), with constant mass flow rate, concentration and temperature. The entrance temperature and concentration are such that, there are no solid particles (crystals) in the solution. The upper and lower copper walls that form the channel are maintained at a cold temperature, $T_{cold}$, and has length equal to $L$. In order to obtain a fully developed flow condition at beginning of the copper wall, there is a plexiglass section at the entrance of the channel, with length equal to $x_d$. Initially, water refrigerating the copper wall flows at the same temperature as the inlet oil, until an equilibrium state is obtained. The test begins, by setting the copper temperature $T_{cold}$ to a value below the wax appearance temperature for the solution, $T_{WAT}$. The deposition occurs when the oil temperature reaches a value lower than the wax appearance temperature, $T_{WAT}$.

The working fluid is a binary homogeneous solution of oil, the solvent, and wax, the solute. The mixture behaves as a Newtonian fluid if the temperature is above the $T_{WAT}$, and as a non-Newtonian fluid below it. At the present work, the rheological fluid properties were measured at the laboratory and adjusted to three different non-Newtonian models: Bingham, Herschel-Bulkley, and a new model for thixotropic fluid (Souza Mendes, 2009). The first two models were selected since they are often encountered in the literature aiming to reproduce the non-Newtonian behavior of the mixture below the wax appearance temperature for the solution, $T_{WAT}$. However, recent measurements (Marchesini et al, 2011) showed a better fit of the rheological parameters by employing the thixotropic model.

## 2. MATHEMATICAL MODEL

To simulate the wax deposition process, a two-dimensional model was developed. The computational domain, shown in Fig. 2, was defined to reproduce the experimental setup, where symmetry in relation to the horizontal axis was enforced. Since the heat losses to the ambient are expected to be small, the entrance plexiglass regions was considered as adiabatic wall. The copper wall temperature was measured and imposed as boundary condition. It is approximately constant and near the cold water temperature $T_{cold}$.

The wax deposition is determined by the solution of the conservation equations of mass, momentum, energy and wax concentration of the mixture. Due to the wax deposition process, the flow cross section area varies, thus the conservation equations are solved in a coordinate system that adapts to the geometry contour, ($\xi$, $\eta$) as shown in Fig. 2. When there is an interface movement, the coordinate system presents a displacement velocity, $\mathbf{U}g = u_g\,\mathbf{i} + v_g\,\mathbf{j}$, where the Cartesian components are $u_g = \partial x/\partial\tau$ and $v_g = \partial y/\partial\tau$.

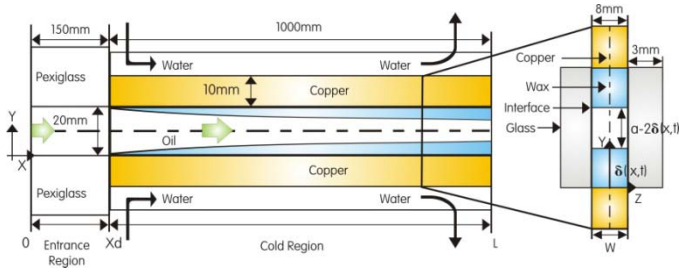


a) full domain b) side view

Figure 1. Schematic view of the test section

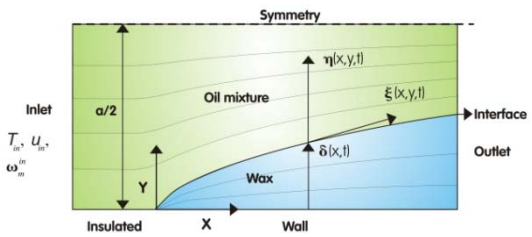


Figure 2. Computational domain and coordinate system

The coordinate system adopted is such that $\vec{e}_\xi$ is tangent to the deposit interface and $\vec{e}_\eta$ .is aligned with the vertical direction, so that

$$\vec{e}_\xi = \frac{\partial\delta}{\partial x}\vec{e}_x + \sqrt{1-\left(\frac{\partial\delta}{\partial x}\right)^2}\,\vec{e}_y \quad ; \quad \vec{e}_\eta = \vec{e}_y \quad ; \quad \xi = \frac{x-x_d}{L+x_d} \quad ; \quad \eta = \frac{y-\delta}{a/2-\delta} \quad ; \quad \tau = t \tag{1}$$

The conservation equations of mass and linear momentum for the liquid phase are

$$\mathbf{div}\ \tilde{\mathbf{U}} = 0 \quad ; \quad \partial(\rho_m\,\mathbf{U})/\partial t + \mathbf{div}(\rho_m\,\tilde{\mathbf{U}}\,\mathbf{U}) = -\,\mathbf{grad}\ p + \ \mathbf{div}\ \boldsymbol{\tau} \tag{2}$$

where

$$\boldsymbol{\tau} = \eta\,(\dot{\gamma})\,2\,\mathbf{D} \qquad \text{and} \quad 2\,\mathbf{D} = \mathbf{grad}\ \mathbf{U} + \ (\mathbf{grad}\ \mathbf{U})^{\mathrm{T}} \tag{3}$$

$\rho_m$ and $\mu$ are the mixture density and absolute viscosity. $p$ is the thermodynamic pressure, $\boldsymbol{\tau}$ is the viscous tensor and $\mathbf{D}$ is the deformation rate tensor. $\tilde{\mathbf{U}}$ represents the velocity vector relative to the ($\xi$ , $\eta$) coordinates and $\mathbf{U}$ is the absolute velocity vector. These are related by $\tilde{\mathbf{U}}$ = $\mathbf{U}$ - $\mathbf{U_g}$, where $\mathbf{U_g}$ is the velocity vector due to the interface movement.

The viscosity of a Bingham and Herschel-Bulkley fluid can be defined as (Soares et al, 1999)

$$\begin{aligned} &\eta\,(\dot{\gamma}) = \frac{\tau_o(T)}{\dot{\gamma}} + \eta_\infty(T) \quad \textit{if} \quad \tau > \tau_o(T) \quad (\text{or} \quad \dot{\gamma} > \dot{\gamma}_{smal}) \\ &\dot{\boldsymbol{\gamma}} = 0 \qquad\qquad \textit{if} \quad \tau \le \tau_o(T) \quad (\text{or} \quad \dot{\gamma} \le \dot{\gamma}_{smal}) \end{aligned} \tag{4}$$

where $\dot{\boldsymbol{\gamma}}$ is the modulus of $\mathbf{D}$, $\dot{\gamma}_{small}$ is the minimum deformation rate associated with yield stress ($\dot{\gamma}_{small} = \tau_o/1000$), and $\eta_\infty$ is the Newtonian viscosity

$$\eta_\infty(T) = \left[k_o(T)\dot{\boldsymbol{\gamma}}^{n-1}\right] \quad ; \quad \dot{\boldsymbol{\gamma}} = \sqrt{2\,\mathbf{D}:\mathbf{D}} \tag{5}$$

$k_o(T)$ and $n$ are the consistency index and exponent parameter. For a Bingham fluid the exponent $n$ parameter is equal to unit. For a Newtonian fluid, $\tau_o$ = 0 and $n$ =1. For both non-Newtonian models, the jellification model consisted in considering that the wax paraffin had became a deposit when $\tau \le \tau_o$, since $\dot{\boldsymbol{\gamma}}$ = 0.

The third rheological model tested is a new thixotropic fluid model developed by Souza Mendes (2009). The steady-state viscosity function of the model is

$$\begin{aligned} &\eta(\dot{\gamma}) = \left[1-\mathbf{exp}\left(-\frac{\eta_o\dot{\gamma}}{\tau_o}\right)\right]\times\left\{\frac{\tau_o-\tau_{od}}{\dot{\gamma}}\,\mathbf{exp}\left(\frac{\dot{\gamma}}{\dot{\gamma}_{od}}\right)+\frac{\tau_{od}}{\dot{\gamma}}+k_o\,\dot{\gamma}^{n-1}\right\}+\eta_\infty \quad \text{if} \quad \dot{\gamma} > \dot{\gamma}_{small} \\ &\dot{\boldsymbol{\gamma}} = 0 \qquad\qquad \text{if} \quad \dot{\gamma} \le \dot{\gamma}_{small} \end{aligned} \tag{6}$$

where $\tau_o$ is the static yield stress, $\tau_{od}$ the dynamic yield stress, $\dot{\gamma}_{od}$ a shear rate that marks the transition in stress from $\tau_o$ to $\tau_{od}$ , $k_o$ is the consistency index, $n$ the power-law index, $\eta_o$ and $\eta_\infty$ are the limiting $\eta$ values corresponding to $\dot{\gamma} \to 0$ and $\dot{\gamma} \to \infty$ , respectively. $\eta_\infty$ can be considered as the Newtonian viscosity. This model has innumerous parameters that must be adjusted with the experimental data. For this case, the jellification model was based on $\dot{\gamma}_{small}$ , i.e., it was considered that the wax paraffin had became a deposit when $\dot{\boldsymbol{\gamma}} \le \dot{\gamma}_{small}$ .

The conservation equation for the mixture concentration $\omega_m$ is only solved in the liquid region

$$\frac{\partial(\rho_m\,\omega_m)}{\partial t} + \mathbf{div}(\rho_m\,\tilde{\mathbf{U}}\,\omega_m) = \ \mathbf{div}\,[(\rho_m\,\mathcal{D}_{mol}\,)\,\mathbf{grad}\,\omega_m\,] \tag{7}$$

where $\mathcal{D}_{mol}$ is the molecular diffusion coefficient.

The properties of the liquid and solid phases were considered identical, therefore, the energy conservation equations for both liquid and solid regions are:

$$\partial(\rho\,T)/\partial t + \mathbf{div}(\rho\,\tilde{\mathbf{U}}\,T) = \ \mathbf{div}\,[(k/c_p)\,\mathbf{grad}\,T\,] \tag{8}$$

where $k$ and $c_p$ are the thermal conductivity and specific heat, and $T$ is the temperature. Note that, because of the

displacement of the coordinates, and the interface movement, it is necessary to introduce a convective term in the energy equation for the solid region, where **U** = 0.

To solve the set of equations (2), (7) and (8), the following boundary conditions were considered: uniform inlet velocity $u_{in}$, temperature $T_{in}$ and mixture wax concentration $\omega_m^{in}$ , and negligible diffusion at the outlet. At the upper boundary a symmetry condition was defined. The entrance wall region was considered adiabatic, and a cool measured temperature was specified at the copper test section wall, $T_{cold}$. At the liquid-wax interface, continuity of heat flux and temperature are enforced. With respect to the flow equations, Eq. (2), no slip condition was imposed at the solid walls (inlet wall region and liquid-wax interface). The interface mixture concentration $\omega_m^{in}$ was specified from the oil-wax solubility curve whenever $T_{int} < T_{WAT}$, otherwise, the interface was considered impermeable (i.e., zero mass flux). The solubility curve $\omega_{sol}$ was experimentally determined by Palomino (2010) as

$$\omega_{sol} = 6.747 \times 10^{-3}\, T^{0.107} \tag{9}$$

where the temperature $T$ is expressed in Celsius.

At the beginning of the process, the copper wall temperature is the same as the inlet oil-wax solution temperature. Thus, at $t$= 0, the interface temperature $T_{int}$ is larger than $T_{WAT}$, therefore both $\delta$ and $d\delta/dt$ are zero.

The growth of the deposited layer was determined with a molecular diffusion mechanism. The diffusion mechanism was accounted as suggested by Burger *et al.* 1981, i.e., the diffusion flux of wax toward the cold wall was estimated by employing Fick's law of diffusion, whenever $T_{int} < T_{WAT}$,

$$\frac{\partial\, m_{wax}}{\partial\, t} = -\rho_m\, \mathcal{D}_{mol}\, A_d\, \frac{\partial\, \omega_m}{\partial\, n}\bigg|_{int} \quad ; \qquad m_{wax} = \rho_{wax}(1-\phi)\, A_d\, \delta \tag{10}$$

where $\rho_m$ is the mixture density, $\mathcal{D}_{mol}$ is the molecular diffusion coefficient, $\omega_m$ is the wax concentration of the mixture (or volume fraction of wax in the solution), $A_d$ is the superficial deposit area, $m_{wax}$ is the wax mass deposited, $\rho_{wax}$ is the solid wax density and $\phi$=$m$/($m$+$m_{wax}$) is the porosity of the oil-filled wax deposit. Combining the equations above, the wax deposition thickness can be obtained from,

$$\frac{\partial \delta}{\partial t} = \frac{-\mathcal{D}_{mol}}{(1-\phi)} \frac{\rho_m}{\rho_{wax}} \left( \frac{\partial \omega_m}{\partial n} \right)_{int} \tag{11}$$

where $\partial\omega_m/\partial n)_{int}$ is the gradient in the normal direction of deposition wax concentration at the interface.

By defining the following dimensionless variables

$$\mathbf{U} = \frac{\mathbf{u}}{u_{in}} \;;\; \mathbf{X} = \frac{\mathbf{x}}{D_h} \;;\; \lambda = \frac{t}{D_h / u_{in}} ;\; P = \frac{p}{\rho_m\, u_{in}^2} \;;\; \theta = \frac{T - T_{WAT}}{T_{in} - T_{WAT}} \;;\; \eta^* = \frac{\eta}{\eta_\infty} \tag{12}$$

where $\eta_\infty$ is the Newtonian viscosity, $D_h$ = 2 a is the hydraulic diameter, it can be shown that in addition to the specific rheological parameters of each model, the problem is governed by the Reynolds number **Re**, Prandtl **Pr** and Schmidt **Sc** numbers, the initial wax concentration $\omega_m^{in}$ and cold cooper temperature $\theta_{cold}$ , as well as the solubility curve (Eq. 9).

$$\mathbf{Re} = \frac{\rho_m\, u_{in}\, D_h}{\eta_\infty} ;\; \mathbf{Pr} = \frac{\eta_\infty\, c_p}{k} \;;\; \mathbf{Sc} = \frac{\eta_\infty}{\rho_m\, \mathcal{D}_{mol}} \;;\; \omega_m^{in} ; \qquad \theta_{cold} \tag{13}$$

## 3. RHEOLOGICAL PROPERTIES

A pretreated laboratory waxy-oil mixture with 15% of wax weight was used to carry out the rheological measurements. The pretreatment consisted on heating the solution at 60ºC. The pretreated wax-oil solution was separated and stored in closed bottles. Before each rheological measurement a sample of one bottle was heated at 50ºC for 30 minutes to erase the oil "memory" by redissolving the wax crystals.

The rheological characterization was performed in a AR-G2 rheometer from TA instruments, with smooth and cross hatched parallel plates and a range of gaps from 0.5 to 3 mm. The set of tests performed included temperature ramps, with the oil being cooled down from 50ºC to 4ºC under a constant cooling rate of 4ºC/min at constant shear rate of 200 $s^{-1}$. It is important to highlight that $T_{WAT}$ is measured by rheometer methodology. The viscosity measured as a function of temperature during cooling and heating is shown in Fig. 3, where it can be clearly seen that the wax appearance temperature is 29 ºC. An interesting observation of the data obtained is the different viscosity behavior during cooling and heating, showing that the wax particles are absorbed by the solution in a different temperature than they leave the solution.

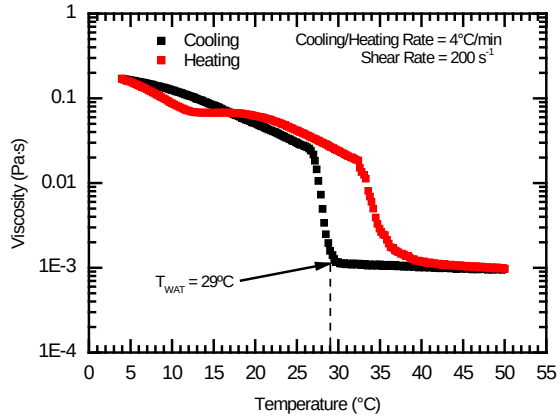


Figure 3. Viscosity as function of temperature during cooling and heating process (4 ˚C/min).

The shear stress and viscosity were also measured, at several different constant temperatures, with varying shear rate (Fig. 4). The Newtonian behavior can be seen that at 40 °C, which is above $T_{WAT}$ (29°C), with constant viscosity. Below $T_{WAT}$, the viscosity increases with temperature and the wax-oil mixture presents a non-monotonic flow curve . The limiting $\dot{\gamma}_{small}$ needed for Thixotropic model was set at 0.1 $s^{-1}$, since it corresponds to the inflection point of experimental data in shear stress curve flow (Figure 4a).

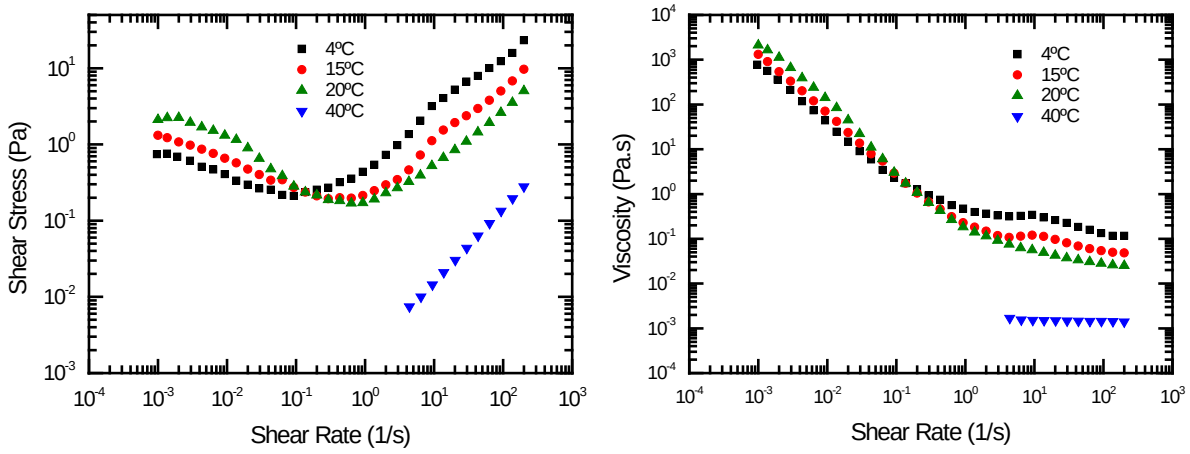


a) Shear stress b) Viscosity

Figure 4. Experimental Flow Curve for 4ºC, 15ºC, 20 ºC and 40ºC, wax-oil mixture at 15% wax concentration.

Figure 5 illustrates the yield stress $\tau_o$ and consistent index $k_o$ temperature dependence adjusted from the measured data. Above $T_{WAT}$, $k_o$ is approximately constant, since the fluid behaves as Newtonian, and below it, $k_o$ varies exponentially. A clear dependence of the yield stress in the temperature below $T_{WAT}$ can also be seen. As the temperature decays, larger values of $\tau_o$ are obtained leading to an increase on the deposit thickness when $\tau < \tau_o$.

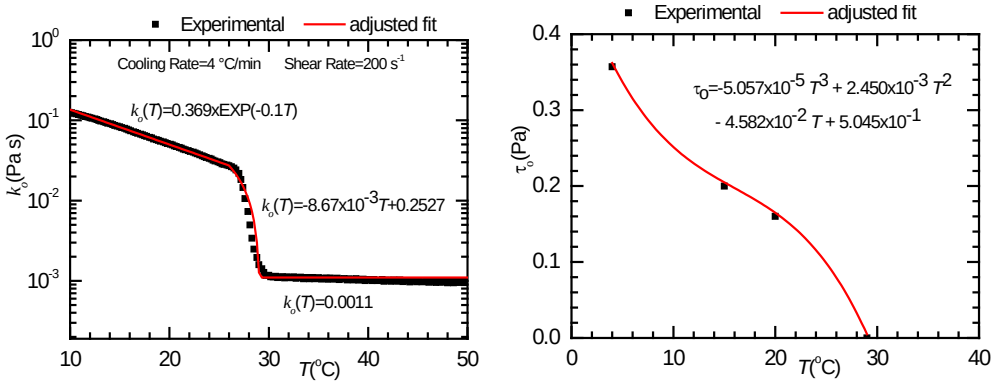


a) Consistency index $k_o$ b) Yield stress, $\tau_o$

Figure 5. Temperature dependency of consistency index $k_o$ and yield stress $\tau_o$

The fitting curve of Bingham, Herschel-Bulkley and Thixotropic models are shown in Figure 6. The Bingham and Herschel-Bulkley do not represent well the experimental data, because the behavior of the Shear Stress flow curve is non-monotonic, and both models are monotonic. However, the Thixotropic represents quite well the non-monotonic curve behavior. The adjusted parameters of Eq.6 with experimental data are shown in Table 1.

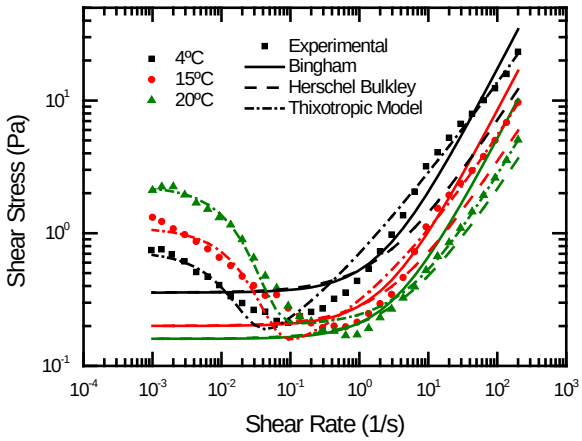


Figure 6. Fit curve for Bingham, Herschel-Bulkley and Thixotropic models.

Table 1. Adjusted parameters of the Thixotropic model for 4ºC, 15ºC and 20 ºC.

| | **4 °C** | **15 °C** | **20 °C** |
|---|---|---|---|
| $\eta_o$ | 7.02E+09 | 6.92E+04 | 1.02E+04 |
| $\tau_o$ | 7.32E-01 | 1.10E+00 | 2.29E+00 |
| $\tau_{od}$ | 8.99E-02 | 9.67E-02 | 2.01E-01 |
| $\dot{\gamma}_{od}$ | 1.15E-02 | 2.03E-02 | 1.73E-02 |
| $k_o$ | 5.86E-01 | 1.90E-01 | 3.83E-02 |
| $n$ | 6.26E-01 | 5.70E-01 | 8.71E-01 |
| $\eta_\infty$ | 1.10E-03 | 1.10E-03 | 1.10E-03 |

## 4. NUMERICAL METHOD

The numerical method selected for solving the set of governing and auxiliary equations was the finite volume method (Patankar 1980) with fully implicit time integration. The fluxes at the control volume faces were determined with the Power-Law scheme. The dependent variables in the linear momentum conservation equation were the contravariant velocity components (normal to the coordinate surface/line) (Pires and Nieckele, 1994), which were stored staggered from the scalar variables, to avoid oscillatory solutions. The pressure-velocity coupling was handled by an algorithm based on SIMPLEC. The resulting algebraic system was solved by the TDMA line-by-line algorithm (Patankar 1980) and a block correction algorithm was employed to speed convergence. The equations of conservation of mass, linear momentum and wax mixture concentration were solved only in the liquid region. The energy equation was solved in the entire domain, in both solid and liquid regions.

The viscosity data for the Thixotropic model as a function of temperature was interpolated. For temperature between 15 and 20˚C , a Newton interpolation scheme using three points (4, 15 and 20˚C) was employed and a linear interpolation for temperature between 20 to 29 ˚C..

In the resolution of phase change problems, the position of the interface is part of the solution, resulting in a more complex algorithm, since the size of the solid and liquid regions change with time. It is assumed that the movement of the fluid inside channel is not strongly influenced by the movement of the interface. Therefore, for each time interval, temperature, mixture concentration and velocity fields can be solved maintaining a fixed solid/liquid interface.

Due to the interface movement, the computational mesh is generated each time the interface changes position. However, since the interface movement occurs only in the vertical direction, the horizontal mesh is maintained constant. The mesh is concentrated near the interface. The mesh distribution of 176 × 99 nodal points, in the vertical and horizontal direction, was defined based on grid tests. A comparison of the thickness of the deposit employing a mesh with 176 x 150 grid and 116 × 69 grid resulted in differences smaller than 2%. At the beginning of the process, 11 points are specified at the solid region, whose width is equal to 0.0025 a. The final number of points in this region depends on the interface displacement. A time step of $10^{-8}$ seconds was specified. The convergence criterion consisted on requiring a residue inferior to $10^{-6}$ for all conservation equations

## 5. RESULTS

To investigate the influence of the non-Newtonian models in the deposition rate, the experimental apparatus shown in Fig. 1, was numerically modeled, aiming to reproduce the experiment. Since the copper temperature was cooled by a water bath, its temperature was measured, and it was realized that due to the wall heating capacity, it was not constant as desired. Therefore, the cooper wall temperature distribution shown in Fig. 7 was imposed as boundary condition for all simulations.

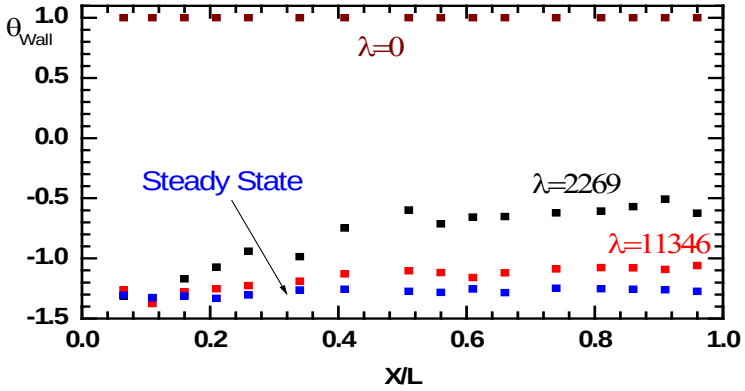


Figure 7 – Experimental wall temperature distribution along the channel, at different time instants.

Three non-Newtonian models (Bingham, Herschel-Bulkley and Thixotropic) were tested and the results obtained were compared with a Newtonian fluid model. For all cases investigated the molecular diffusion was considered as the deposition mechanism. For the non-Newtonian cases, additional deposition mechanism represented by the paraffin jellification was considered. The same consistent index and yield stress as shown in Fig. 5 were specified for the Bingham and Herschel-Bulkley model. For the later, the *n* exponent was set as 0.8. The Thixotropic parameters are shown in Table 1.

The test case selected to be presented here corresponds to Reynolds number is equal to 1732, and the Prandtl and Schmidt numbers equal to 13.9 and 1433, respectively. The inlet wax concentration $\omega_{in}$ is equal to 15% and the dimensionless cold temperature was $\theta_{cold}$= –1.273. These are typical values for the oil-wax mixture employed in the laboratory tests. The results obtained with the different models are compared with the experimental data (Palomino, 2010).

Figure 8 presents the axial distribution of the deposition thickness within the channel at steady state. At steady state, all rheological models predicted the same deposition thickness, since at the interface the temperature is equal to the $T_{WAT}$, a value above which there is no more deposition. The agreement is very good at the beginning of the cool copper plate with differences inferior to 5%, but it deteriorates as one move along the channel, reaching the maximum difference of 25%.

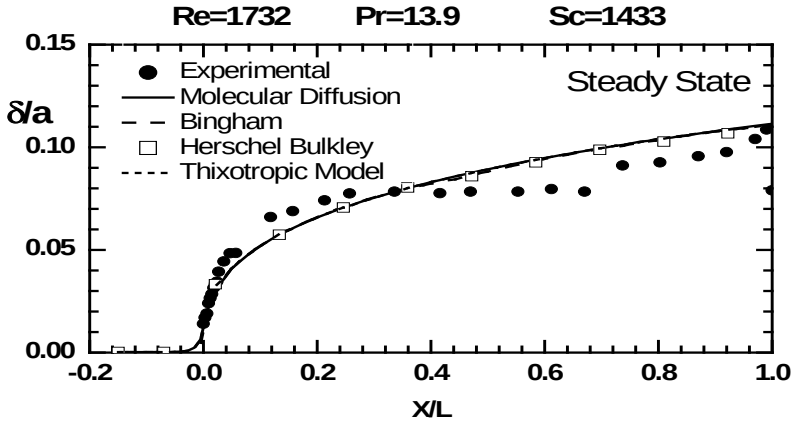


Figure 8 – Deposition thickness at distribution along the channel at steady state

The influence of the jellification deposition mechanism based on the non-Newtonian behavior of the fluid can be appreciated during the transient regime. Figure 9 presents the deposit thickness distribution along the channel for three different time instants, corresponding to the dimensionless time λ equal to 2269, 5673 and 11346. Examining Fig. 9, it can be clearly seen that the Molecular Diffusion Mechanism underestimates the deposit thickness during the transient, especially at the first time instants. This fact indicates that Molecular Diffusion is not the only relevant deposition mechanism. It can also be seen that the inclusion of a jellification model improves substantially the deposit thickness prediction. However, it is not completely clear which non-Newtonian model is more adequate, but the Bingham model seems to be a little superior to the other two. In spite of the better rheological adjustment of the thixotropic model, it

does not produce the better thickness prediction. The main reason can be attributed to the threshold value of $\dot{\gamma}_{small}$ employed to imply that the wax had solidified. Further, this model was more unstable, causing some unrealistic waviness on the deposit surface.

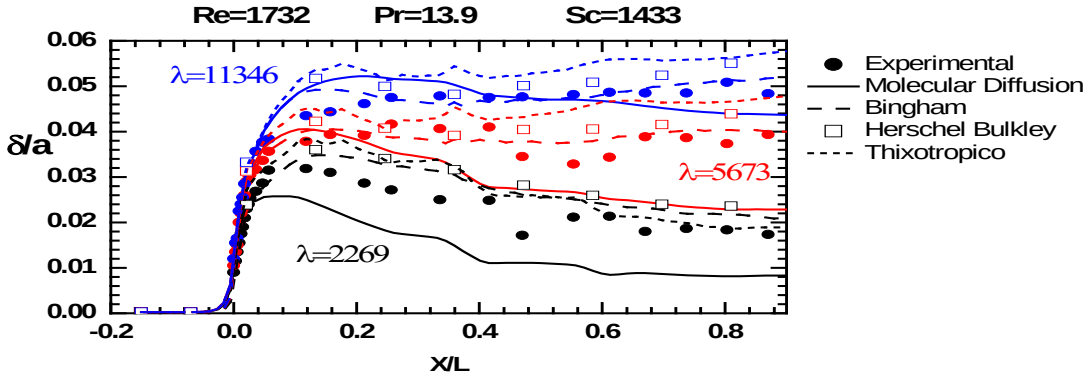


Figure 9 – Deposition thickness at distribution along the channel, at different time instants.

Figure 10 presents temperature and velocity distribution across the channel, at three different axial stations for dimensionless time $\lambda$ = 2269. All three non-Newtonian models predicted very similar velocity and temperature distribution. Note in Fig. 10a, the increasing thickness of the temperature boundary layer. A fully developed velocity profile can be seen, which is also smoother, since the Reynolds corresponds to a laminar regime. The differences between the temperature and velocity profile predicted by the non-Newtonian models and the Newtonian case (only Molecular diffusion deposition mechanism) are basically due to the different deposit thickness.

The yield stress increases when the temperature decreases for both Bingham and Herschel-Bulkley model. Therefore, higher yield stress values prevail at the region near the cold wall. Thus, near the wall the yield stress $\tau_o$ is larger than the shear stress imposed by the flow. As a consequence, the fluid stops flowing and the wax becomes a gel increasing the deposit thickness. Further, as the fluid flows along the channel, it is cooled by the cooper wall, resulting in lower temperatures at the end of the channel, which will cause an enhancement of the deposit due to the higher yield stress. The increase on the deposit thickness obtained with the Thixotropic model is mainly due to the substantial increase of the apparent viscosity.

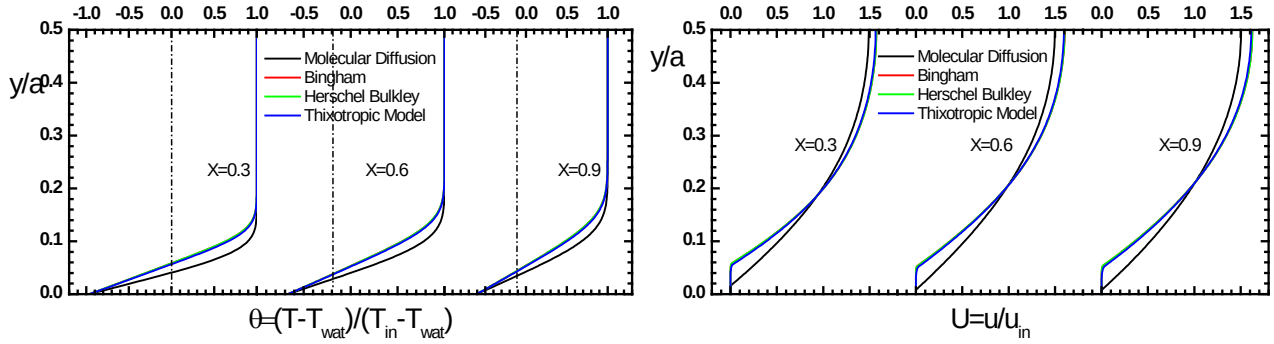


(a) temperature (b) velocity

Figure 10 – Temperature and velocity profiles at three axial stations, at dimensionless time λ = 2269

The interface temperature distribution along the channel is illustrated in Figure 11 for all cases studied, for different time instants. As the fluid flows along the channel, it is cooled by the cooper wall, and lower temperatures are found near the exit section of the channel. At the begging of the process, the cold wall cools the fluid, freezing the flow since the shear stress is smaller than the large yield stress. As time passes, the deposit thickness increases and the deposit works as an insulator, preventing the fluid temperature to drop. When the interface temperature approaches $T_{WAT}$, deposition ceases to occur.

The wax deposit thickness is plotted in Fig. 12a as a function of time, for all cases, at same three axial stations (near the entrance, half and near the exit) as the temperature and velocities (Fig. 10). Examining Figure 12a, two distinct deposition growth behaviors can be identified for the three non-Newtonian models. In the first region, the deposition is strongly influenced by the non-Newtonian behavior of the fluid, which freezes the flow. When the interface temperature approaches the wax appearing temperature $T_{WAT}$, the yield stress goes to zero and the fluid behaves as Newtonian, thus molecular diffusion prevails as the driving mechanism for wax deposition. If the cooling rate is slow the dominate deposition process is the Molecular Diffusion but if it is fast, the dominate deposition process is non Newtonian gel deposition.

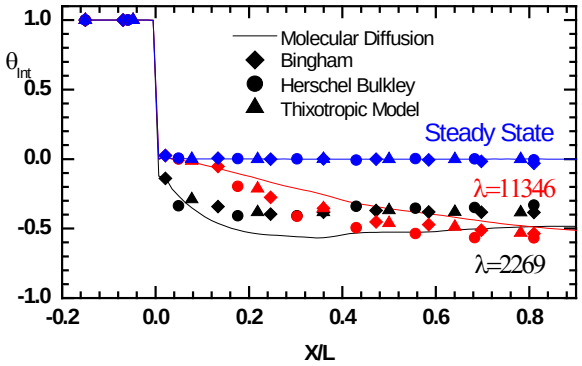


Figure 11 – Interface temperature distribution along the channel, at different time instants.

The total mass deposited can be defined normalized by the maximum amount of mass that can be deposited in the channel $m_{dmax}$ as

$$m_d^* = m_d / m_{d\,max} = 2\int_0^1 (\delta / a)\, dX \tag{14}$$

The time variation of the total mass deposited can be seen in Figure 12b, as a function of different rheological models. Note that, the three models have the same wax deposited. A stronger increase in the wax deposited can be seen during the beginning of the process. Since the deposition only occurs when $T < T_{WAT}$, and the rheological behavior also only influences the flow in this situation, the steady state regime is independent of the models, as already discussed.

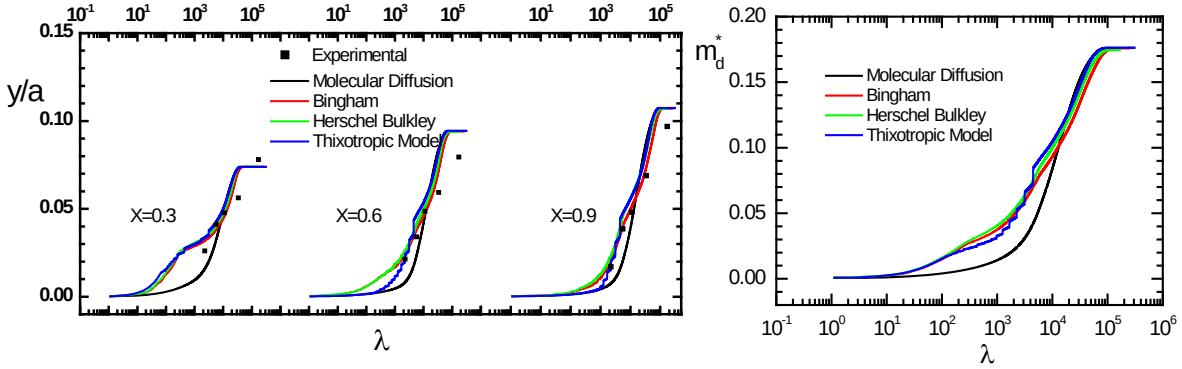


(a) At three positions along the channel. (b) Total mass deposited

Figure 12 – Time variation of the deposit thickness at

## 6. CONCLUSION

The present paper investigated the influence of jellification mechanisms in addition to the molecular diffusion mechanism to predict the wax deposition phenomena. To this end, a simulation was performed and the deposition thickness was compared with experimental data obtained from a control experiment in a channel, designed to study wax deposition mechanism. Three models were selected to be investigated. They combine a molecular-diffusion-based mechanism with a non-Newtonian behavior of the fluid flowing at temperatures below the wax appearance temperature. The wax-oil mixture was modeled as Bingham, Herschel-Bulkley fluids, with a temperature dependent yield stress and viscosity. It was also modeled as a thixotropic fluid with a dynamic Yield Stress that corresponds to small shear rate ($0.1\ s^{-1}$).

As already shown in several works, the steady state deposit thickness is independent of the deposition mechanism. However, the results obtained indicated that the additional deposition mechanism due to jellification improved the deposit thickness prediction during the transient regime, by producing thicker deposit due to the gel formation of the mixture close to the channel cold wall. The contribution of non-Newtonian gel deposition mechanism is more significant at the beginning of the cooling process, due to the presence of lower temperatures which lead to higher yield stress. Further, due to smaller temperatures found near the channel exit, the jellification mechanism also increases the deposit in this region in relation to only considering the Molecular Diffusion model.

In spite of the rheological characterization of the fluid and the better adjustment for the rheological parameters obtained with the thixotropic models, no model presented a significant better prediction with regards to the deposition thickness.

7. **ACKNOWLEDGMENTS**

The authors gratefully acknowledge the support awarded to this research by the PETROBRAS Research Center – CENPES, the Brazilian Research Council – CNPq, Rio de Janeiro State Research Foundation, FAPERJ, and the Fund for Research and Development in Petroleum – CTPetro

## 8. REFERENCES ACKNOWLEDGMENTS

Vinay, G., Wachs, A., Agassant, J.F., 2005, "Numerical simulation of non-isothermal viscoplastic waxy crude oil flows ", Journal of Non-Newtonian Fluid Mechanics, 128, 144-162

Azevedo L.F.A., Teixeira A.M., 2003, "A critical review of the modeling of wax deposition mechanisms". Petrol Sci Technol 21, (3 and 4), 393–408.

Benallal, A., Maurel, P., Agassant, J.F., Darbouret, M., Avril, G., Peuriere, E., 2008, "Wax deposition in pipelines: Flow-Loop experiments and investigations on a novel approach", Annual Technical Conference of the Society of Petroleum Engineers paper no. 115293.

Brown,T.S., Niesen, V.G. and Erickson, D.D., 1993, "Measurement and Prediction of the Kinetics of Paraffin Deposition", 68th Annual Conference of the Society of Petroleum Engineers paper no. SPE 26548.

Burger, E.D., Perkins, T.K. and Striegler, J.H., 1981, "Studies of Wax Deposition in the Trans Alaska Pipeline", Journal of Petroleum Technology, 33, 1075-1086.

Correra,S.;·Fasano, A.; Fusi, L; Merino-Garcia, D, 2007, "Calculating Deposit Formation in the Pipelining of Waxy Crude Oils", Meccanica, 42, 149–165.

Fasano, A., Fusi, L., Correra, S., 2004, "Mathematical Models for Waxy Crude Oils ", Meccanica, 39, 441-482.

Fusi, L., 2003, "On the Stationary Flow of a Waxy Crude Oil with Deposition Mechanisms", Non Linear Analysis, 53, 597-526.

Ghanaei, E. and Mowla, D., 2010, "Prediction of Waxy Oil Rheology by a New Model", Energy & Fuels, 24, 1762-1770.

Hoteit, H., Banki, R., Firoozabadi, A., 2008, "Wax Deposition and Aging in Flowlines from Irreversible Thermodynamics", Energy & Fuels, 22, 2693–2706.

Marchesini, F.H. De Souza Mendes, P.R., Nieckele, A.O., Azevedo, L.F.A, Trampus, B.C., Minchola, L.R., 2011, “Postcooling flow properties of a model w axy crude oil”, AERC 2011, 7th Annual European Rheology Conference, Suzdal - Russia

Mehrotra, A.K. and Bhat, N.V., 2007, "Modeling the Effect of Shear Stress on Deposition from “Waxy” Mixtures under Laminar Flow with Heat Transfer", Energy & Fuels, 21, 1277-1286.

Merino-Garcia, D., Margarone, M., Correra, S., 2007, "Kinetics of Waxy Gel Formation from Batch Experiments", Energy & Fuels, 21, 1287-1295.

Minchola, L. R., Nieckele, A.O. and Azevedo, L.F.A., 2007, "Numerical Simulation Of Wax Deposition In Channel Flow", Proceedings of the 19th International Congress of Mechanical Engineering, Brasília, DF, Brazil, paper 2085.

Minchola, L. R., Nieckele, A.O. and Azevedo, L.F.A., 2008, "Modeling wax deposition in channel flow with Molecular and Brownian diffusion models", Proceedings of the V National Congress of Mechanical Engineering, Salvador, BA, Brazil, Paper CON08-0831.

Minchola, L.R., Nieckele, A.O., Azevedo, L. F. A., 2010, "The influence of rheological parameter in wax deposition in channel flow", Proceedings of the International Heat Transfer Conference IHTC14 – 22952.

Palomino, L.F., 2010, "Experimental investigation of wax deposition in turbulent channel flow", Master’s dissertation, Dept. Mechanical Engineering, PUC-Rio (in portuguese)

Patankar, S. V., 1980, "Numerical Heat Transfer and Fluid Flow", McGraw-Hill.

Pires, L. F. G. and Nieckele, A. O., 1994, "Numerical Method For The Solution Of Flows Using Contravariant Components In Non-Orthogonal Coordinates", Proceedings of the V Brazilian Meeting on Thermal Sciences, São Paulo, SP, Brazil, pp. 343-346.

Romero, M.I., Leiroz, A.T., Nieckele, A.O. and Azevedo, L.F.A., 2006, "Evaluation of a Diffusion Based Model to Predict Wax Deposition in Petroleum Pipelines", 13th International Heat and Mass Transfer Conference, Sidney, Australia.

Soares, M., Naccache, M.F, Souza-Mendes, P.R., 1999, "Heat Transfer to Viscoplastic materials flowing laminarly in the entrance region of tubes", International Journal of Heat and Fluid Flow, 20, 60-67.

Souza Mendes, P.R., 2009, "Modeling the thixotropic behavior of structured fluids", Journal of Non-Newtonian Fluid Mechanics, 164, 66-75.

## 9. RESPONSIBILITY NOTICE

The authors are the only responsible for the printed material included in this paper.